Supplementary Information

Contents

1 Further Experimental Data

1.1 Features of stored deformation

Fig. 1 shows images of a sponge of elasticity $E \sim 7MPa$. We show response in the elastic and pseudo-plastic state in Fig. 1(a) and (b) respectively. (a) shows no deformation I_d is stored whereas, on indentation to I_c, as shown in Fig. 1 (b)(ii) and the indentation up to a depth I_d is permanently stored as shown in (b)(iii). Fig. 1(c) shows that small indentation with various indentors can be created on the surface in distinct shapes, which can be thought of as writing multiple bits in parallel and close to each other. Also, as we discussed in the main text that the deformation in the pseudo-plastic state is highly localised, a demonstration of this can be seen in Fig. 1(d). A small hexagonal unit of a few rods is colored blue as shown in (d) (i). It is then indented by a small indentor of diameter 2mm and the state of the colored

unit of rods after indentation is shown in (d)(ii). In our experiments, we also observed that applying strain by compressing on both orthogonal axes perpendicular to the direction of vertical indentation leads to even better retention of the deformed shape. However, most features discussed are present in the case of uniaxial strain. So, we have focused only on the case of uniaxial strain in our experiments.

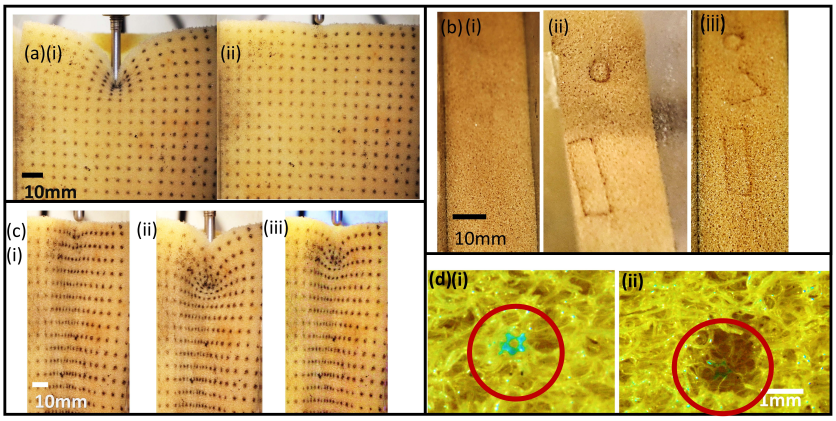

Figure 1: (a)(i) shows the indented elastic state of sponge and (ii) shows that on removal of indenatation, a regular grid printed on the undeformed sponge comes back to it's original state. (b)(i)-(iii) show the sponge in pseudo-plastic state before, during and after indentation respectively. (c) shows various shapes that can be indented via differently shaped indentors. (d) (i)-(ii) show the behaviour of a small blue colored region (circled red) in the pseudo-plastic state before and after indentation as seen with a 10x microscope.

1.2 Reproducible Fluctuations in F_{ind}

In our experiments, we also observed that applying strain by compressing on both orthogonal axes perpendicular to the direction of vertical indentation leads to even better retention of the deformed shape. We discuss the fluctuations in the measured value of F_{ind} here. It was found that small fluctuations in the value of F_{ind} are repeatable in multiple experiments of indentation, when performed at the same location. This reproducibility is demonstrated in Fig. 2. This can be attributed to re-formation of the complex buckled microstructure of the rods. This therefore substantiates the claims of the complete erasure of previously stored deformation on setting $\gamma = 0$.

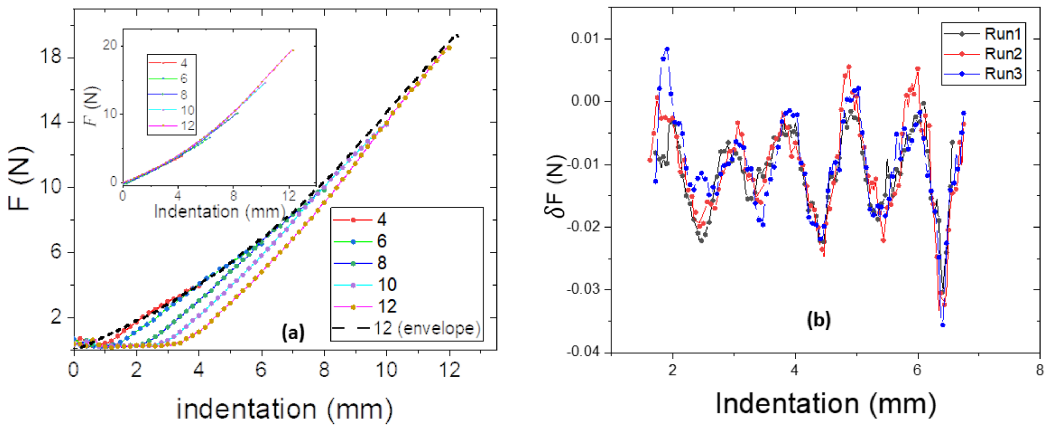

Figure 2: (a) shows only the forward part of indentation cycle for indentation to various depths following protocol $\mathbf{P_2}$. (b) shows $F - F_{avg,T}$ for the indentation force.

1.3 Sponge properties and characterization

Cellular materials have a vast literature discussed in introduction of the main text. These can be broadly classified as open-cell or close cell foams or sponges. The cellular materials discussed in this paper are of open-cell type, i.e., made of rods, while closed-cell sponges are made of walls rather than rods. These materials demonstrate interesting negative Poisson's ratio as demonstrated in Fig.3 (a). Considering $h(x) = 0$ to be the initial profile of the surface where x varies from 0 to L (L being the distance between the compression plates). It goes to a slightly u-shape with $h(x) < 0$ for finite strains. This is typical behaviour known in literature for cellular materials. The rods at the surface are buckled in random orientations and on a coarse scale, the surface is smooth, even though there are minor wrinkles or fluctuations due to buckling of surface rods.

Since these polymeric materials are viscoelastic, there is a time rate at which applied forces decay as seen in Fig.3(b). We see that if compressed at a high strain rate, F_{ind} will relax in time, with a very short timescale. Whereas, at low enough strain rates, relaxation time will be very long, and force relaxation will be negligible. From Fig. 3(c), we find that $\tau \sim 10s, 100s$, i.e., there is a shorter relaxation timescale of 10 seconds and a longer relaxation timescale of 100 seconds. For the slow indentation rates that we use in our experiments, the faster timescale doesn't play a role but the effect of the

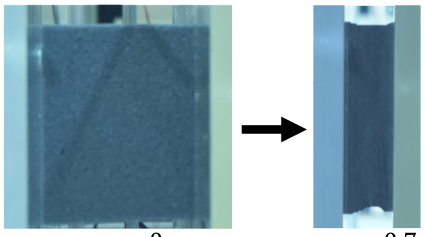

(a) Figure shows that height after compression decreases, implying negative Poisson's ratio.

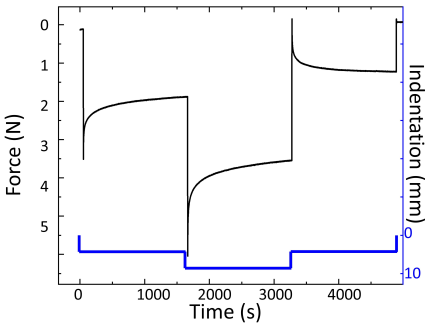

(b) Figure shows the variation of response of sponge in the pseudo-plastic state under fast indentation with time. There are multiple relaxation timescales $\tau \sim 10s, 100s$ here.

Figure 3: Sponge Properties

longer relaxation timescale $\tau \sim 100s$ gives slight viscoelasticity to the elastic phase.

1.4 Variation of I_d vs γ

As we vary the strain γ, we observe maximum I_d that can be stored for the same value of I_c to increase. Results are shown in Fig. 4.

1.5 Variation of indentor

We obtained same results of deformation storage with a different indentor. Fig. 5(a) (i-iv) show the post indentation images with deformation I_d stored in a sponge material compressed between two plates for increasing values of indentation I_c. (b) shows that the indentor is threaded in this case, in contrast to the indentor shown in Fig. 4 of the main text which has a smooth surface.

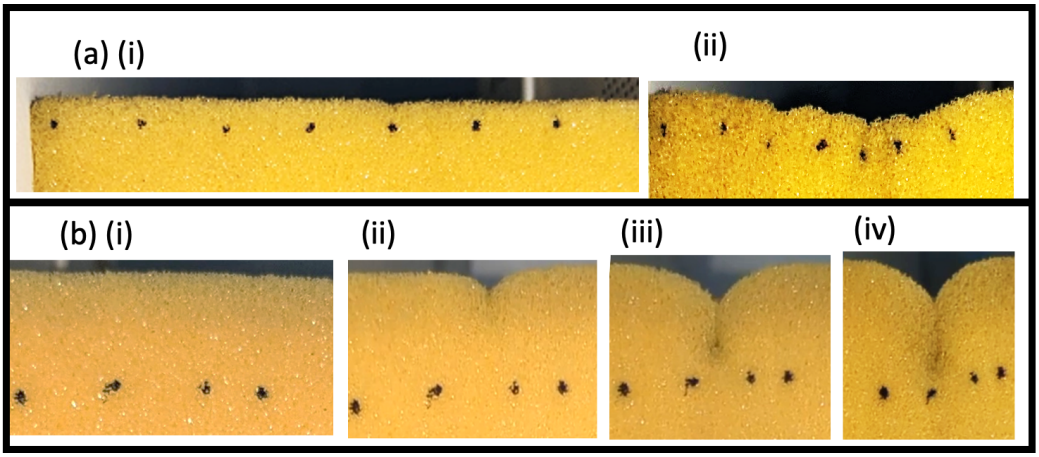

Figure 4: (a) shows the buckled surface under strain in (ii) as compared to the flat surface in (i) without strain. (b) (i)-(iv) show an image after indentation for increasing values of γ representing an increase in I_d, which is the maximum deformation that can be stored, for the same value of I_c.

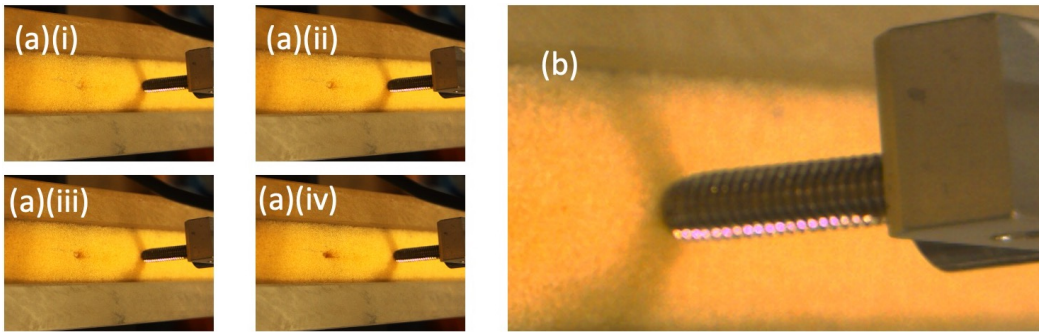

Figure 5: (a) shows deformation I_d stored for increasing values of I_c. (b) shows the threaded indentor.

2 Theoretical Analysis of a single hyper-elastic rod

Here, we discuss the behaviour of a single hyperelastic rod under external force. A single rod will undergo Euler buckling at critical load $n^2\pi^2 EI/L^2$ under normal forces, and at a critical strain ϵ_c as labelled in Fig. 6(a).

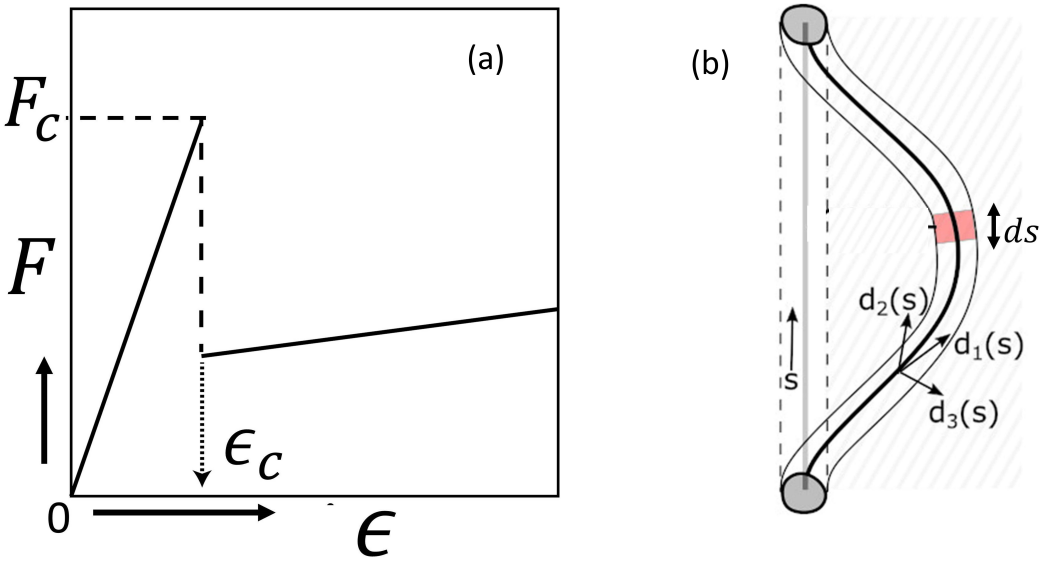

Figure 6: (a) shows the F v/s ϵ curve expected for buckling of a single rod. (b) shows the 3 orthonormal vectors (Serret-Frenet triad) along the length of a single rod parametrized by s

Fig. 6 (b) shows the undeformed configuration of a 3D rod parameterised by arclength s (s varies from 0 to ℓ) along the center of the rod on the 'centerline' in Euclidean R^3 space. At every point s on the rod, we can associate three orthonormal vectors $\vec{d_1}, \vec{d_2}$ and $\vec{d_3}$ which stand for Tangent, Normal and Binormal. Together these are also known as the Serret-Frenet triad. In the deformed condition of the rod shown with the solid line in Fig. 6 (b), the vectors will continue to be orthonormal if we ignore the shearing of the rod (which holds for for thin rods). For uniform deformation, we can account for the stretching, bending and twisting of these rods via the derivatives of the vectors $\vec{d_1}, \vec{d_2}$ and $\vec{d_3}$ along the parameter s. For orthonormal vectors, the derivatives can be broken down to three scalar functions $\kappa^{(1)}(s), \kappa^{(2)}(s)$ and $\tau(s)$ [1]. Here $\kappa^{(1)}, \kappa^{(2)}$ and τ are interpreted as the local rates of rotation of

the Serret-Frenet triad. $\kappa^{(1)}$ and $\kappa^{(2)}$ represent curvature due to bending of the rod along the plane orthonormal to the tangent vector, and tau refers to the twisting of the rod, around the tangent vector. Also, here $\int ds = \ell + d\ell$, and $u = d\ell/\ell$ is the uniform strain in the rod. The energy per unit length for the rod in terms of curvature, twist and strain can be written as

$$\frac{\epsilon_{rod}}{\ell} = \int ds \frac{EI}{2} \kappa^{(1)}(s)^2 + \int ds \frac{EI}{2} \kappa^{(2)}(s)^2 + \int ds \frac{\beta J}{2} \tau(s)^2 + \frac{E\pi r^2}{2} u^2 \quad (1)$$

Here, $I = \pi r^4/4$ and $J = \frac{\pi r^4}{2}$ are moments of bending and twist and β is the mass per unit length. We find that elastic energy and bending energy scale as r^4 whereas stretching energy scales as r^2. This implies that for thin rods, stretching is much more costly, and the stretching restoration forces are much higher than bending restoration forces. Resistance to bending can be thought of as being provided by a spring constant k_t and resistance to stretching is provided by a spring constant k_ℓ[2]. The buckling and the stretching spring constants are related by $k_t/k_\ell = (r/\ell)^2$ which points to an arguement for inextensibility in the rod and a treatment of an individual rod similar to elastica.

3 Simulation

We simulated the behaviour with a visco-elastic model called the Kelvin-Voigt model which has a spring and a dashpot in parallel [3]. As the indentor indents the material, more and more material starts interacting with the indentor as shown in Fig. 3 in the main text. We incorporated this behaviour into the behaviour of the spring constant k.

In the forward cycle, the stress-strain curve, or the $f_{ind} vs x$ curve is given by the following relation:

$$f_{ind} = k_{int} x + \eta \dot{x} \quad (2)$$

On removal of applied stress, the visco-elastic material relaxes it's strain over a timescale $\tau_{eff} \sim \eta/k_{eff}$. Therefore $x = x_c e^{-t/\tau_{eff}}$. The instantaneous force on an indentor experienced by such a relaxation can be given by the same equation 2. In the compressed phase, k will increase linearly with γ as evident from Fig. 2(f) of the main text. In the presence of a frictional force, f_{fric}, the force balance equation can be written as:

$$f_{ind} = k_{int}x + \eta\dot{x} + f_{fric} \tag{3}$$

Friction is a highly non-linear force, and it can take any value while resisting motion along contacts, varying from 0 to a maximum value[4]. In our simulation, we set the direction of f_{fric} to be opposite of $\dot{x}$. Moreover, k_{eff} and f_{fric} depend on I^2 as shown in Fig. 3 of the main text. We have therefore set $k_{eff} \propto x^2$ and $f_{fric} \propto x^2$ in our simulation code. This will result in an equilibrium x_d such that $k_{eff}x_d \approx f_{fric}$. Deformation will be encoded when $\tau_{eff} \to \infty$ which happens when $k_{eff}x_d \approx f_{fric}$. Codes can be found on [5].

References

[1] Basile Audoly and Yves Pomeau. *Elasticity and geometry: from hair curls to the non-linear response of shells*. Oxford university press, 2010.

[2] Harsh Jain, Shankar Ghosh, and Kirti Chandra Sahu. Compression-controlled dynamic buckling in thin soft sheets. *Physical Review E*, 104(3):L033001, 2021.

[3] Allen C Pipkin. *Lectures on viscoelasticity theory*, volume 7. Springer Science & Business Media, 2012.

[4] Shankar Ghosh, AP Merin, and Nitin Nitsure. On the geometric phenomenology of static friction. *Journal of Physics: Condensed Matter*, 29(35):355001, 2017.

[5] Harsh Jain. Reversible Mechanical Imprint, 2024. GitHub repository.